

Probing Primordial Magnetism with Off-Diagonal Correlators of CMB Polarization

Amit Yadav^{1,2}, Levon Pogosian³, Tanmay Vachaspati⁴

¹*Institute for Advanced Study, Princeton, NJ 08540, USA*

²*Department of Physics,*

University of California at San Diego, La Jolla, CA 92093

³*Department of Physics, Simon Fraser University,*

Burnaby, BC, V5A 1S6, Canada

⁴*Physics Department, Arizona State University,*

Tempe, AZ 85287, USA

Primordial magnetic fields (PMF) can create polarization B -modes in the cosmic microwave background (CMB) through Faraday rotation (FR), leading to non-trivial 2-point and 4-point correlators of the CMB temperature and polarization. We discuss the detectability of primordial magnetic fields using different correlators and evaluate their relative merits. We have fully accounted for the contamination by weak lensing, which contributes to the variance, but whose contribution to the 4-point correlations is orthogonal to that of FR. We show that a Planck-like experiment can detect scale-invariant PMF of nG strength using the FR diagnostic at 90GHz, while realistic future experiments at the same frequency can detect 10^{-10} G. Utilizing multiple frequencies will improve on these prospects, making FR of CMB a powerful probe of scale-invariant PMF.

I. INTRODUCTION

Magnetic fields are prevalent in the cosmic structures around us, in galaxies $B \sim 1 \mu\text{G}$ with coherence length $\lambda \sim 1$ kpc, in galaxy clusters $B \sim 1 - 10 \mu\text{G}$ with coherence length $\lambda \sim 10 - 100$ kpc, and in objects at high redshifts $z \sim 2$ with magnetic field $B \sim 10 \mu\text{G}$ [1]. Recently there have also been claims of a lower bound on the inter-galactic magnetic field, $B > 10^{-15}\text{G}$ [2–5], and perhaps a measurement $\sim 10^{-15}\text{G}$ [6], based on the absence of GeV γ -ray emission in the cascade initiated by TeV γ -rays. The claim is under debate as it has been argued that plasma instabilities could also explain the nonobservation of GeV photons [7], though a counterargument that supports the initial claim has been presented in Ref. [8] It is possible that these magnetic fields have a common origin from a “seed” magnetic field imprinted in the early universe (see [9] for a review). Magnetic fields may be generated at cosmic phase transitions [10–17] and through specially engineered inflationary mechanisms [18, 19].

Detection of primordial magnetic fields (PMF) can lead to important insights into fundamental physics and the early universe. Currently, there are upper limits on the strength of PMF from big-bang nucleosynthesis (BBN) [20–24] and the Cosmic Microwave Background (CMB) temperature anisotropies [25–28], including their non-Gaussian statistics, such as bispectrum and trispectrum [29, 30]. Metric fluctuations induced by PMF are intrinsically non-Gaussian because the stress-energy is quadratic in the magnetic field strength \mathbf{B} and thus non-Gaussian distributed even if \mathbf{B} itself is Gaussian. In this paper we study the detectability of PMF through a different observational window, namely, the Faraday Rotation (FR) signal they induce in the CMB polarization [31]. The polarization of the CMB field can be studied in terms of the parity even E and parity odd B -modes [32–34]. FR converts some of the primordial E -modes into B -modes, thus providing a contribution to the B -mode power spectrum along with the weak gravitational lensing and primordial sources, like the actively sought inflationary gravity waves [32, 33, 35] or cosmic strings [36].

Importantly, spatially dependent FR also couples off-diagonal CMB modes, effectively producing additional non-Gaussian signatures in the CMB polarization. The FR induced parity odd correlations $\langle TB \rangle$ and $\langle EB \rangle$ must vanish in a statistically isotropic universe¹, where the ensemble average is over many realizations of the stochastic magnetic field. However, *a particular realization* of the FR distortion field that generates a B -mode from the primordial E -mode will correlate the respective Legendre coefficients E_{lm} and $B_{l'm'}$. In fact, as shown in [39], it is possible to reconstruct the distortion $\alpha(\hat{\mathbf{n}})$ at a given point $\hat{\mathbf{n}}$ on the sky from specially constructed linear combinations of products $E_{lm}B_{l'm'}$. The additional correlations induced by FR also manifest themselves as connected 4-point functions of the CMB, which, in turn, provide a measurement of the distortion spectrum $C_L^{\alpha\alpha}$ [40, 41].

In this paper we discuss the detectability of primordial magnetic fields through estimators based on 4-point correlations $\langle EBEB \rangle$ and $\langle TBTB \rangle$, as well as the 2-point function $\langle BB \rangle$. In particular, we determine which of the estimators

¹ This statement is specific to the FR induced parity-odd two-point correlations, which are quadratic in the magnetic field strength \mathbf{B} . Metric fluctuations sourced by magnetic stress-energy can produce non-zero $\langle TB \rangle$ and $\langle EB \rangle$, which are quartic in \mathbf{B} , if the net helicity in the magnetic field is non-zero [37, 38].

has the highest signal to noise for several types of magnetic field spectra and for a range of experimental sensitivities. We demonstrate that FR will be a very promising diagnostic of primordial magnetic fields. In particular, future generation of sub-orbital or space-based CMB polarization experiments will be able to detect scale-invariant magnetic fields as weak as 10^{-10} G based on the measurement at 90 GHz frequency. Measurements at multiple frequencies can further significantly improve on these prospects.

II. FARADAY ROTATION FROM MAGNETIC FIELDS

Magnetic fields at CMB decoupling will rotate the polarization vector by an angle

$$\alpha = \frac{3}{16\pi^2 e} \lambda_0^2 \int \hat{\tau} \mathbf{B} \cdot d\mathbf{l} , \quad (1)$$

where $\hat{\tau} \equiv n_e \sigma_T a$ is the differential optical depth, n_e is the line of sight free electron density, σ_T is the Thomson scattering cross-section, a is the scale factor, λ_0 is the observed wavelength of the radiation, \mathbf{B} is the ‘‘comoving’’ magnetic field, and $d\mathbf{l}$ is the comoving length element along the photon trajectory. We are using Gaussian natural units with $\hbar = c = 1$, and the integration limits are from the initial to the final position of the photon.

Statistically homogeneous and isotropic primordial seed magnetic fields can be generated in the early universe during phase transitions [10–17], and are described in terms of a two-point correlation function in Fourier space

$$\langle b_i(\mathbf{k}) b_j(\mathbf{k}') \rangle = (2\pi)^3 \delta^{(3)}(\mathbf{k} + \mathbf{k}') [(\delta_{ij} - \hat{k}_i \hat{k}_j) S(k) + i \varepsilon_{ijl} \hat{k}_l A(k)] , \quad (2)$$

where $S(k)$ and $A(k)$, the symmetric and anti-symmetric magnetic power spectra, are real functions of $k = |\mathbf{k}|$. The function $A(k)$ quantifies the amount of magnetic helicity which plays a crucial role in determining the coherence scale and the magnitude of magnetic fields as they evolve from an earlier epoch until decoupling. However, only $S(k)$ appears in the two-point correlation function of the FR angle, which determines the CMB observables evaluated in this paper. As in [42], we introduce the dimensionless ‘‘FR power spectrum’’ defined as

$$\Delta_M^2(k) \equiv k^3 S(k) \left(\frac{3\lambda_0^2}{16\pi^2 e} \right)^2 = \begin{cases} \Delta_0^2 \left(\frac{k}{k_I} \right)^{2n} & 0 < k < k_I \\ \Delta_0^2 \left(\frac{k}{k_I} \right)^{2n'} & k_I < k < k_{\text{diss}} \\ 0 & k > k_{\text{diss}} \end{cases} , \quad (3)$$

where

$$\Delta_0^2 \equiv \frac{9n}{16\pi e^2 \kappa} \rho_\gamma \lambda_0^4 \Omega_{B\gamma} \approx 1.1 \times 10^4 \frac{\Omega_{B\gamma}}{\kappa} \times \left(\frac{2n}{5} \right) \left(\frac{90 \text{ GHz}}{\nu_0} \right)^4 .$$

This form of the symmetric magnetic spectrum is based on the numerical simulations of causal magnetic field evolution in [43]. In the above, ρ_γ is the comoving photon energy density, $\Omega_{B\gamma}$ is the magnetic energy density relative to the photon energy density, k_{diss} is a dissipation scale above which magnetic fields dissipate, k_I is an intermediate inertial scale, and

$$\kappa = 1 + \frac{n}{n'} \left\{ \left(\frac{k_{\text{diss}}}{k_I} \right)^{2n'} - 1 \right\} . \quad (4)$$

All variables, unless explicitly stated, are in comoving coordinates. The exponents $n = 5/2$ and $n' = 3/2$ correspond to causal magnetic fields [43], and $n \approx n' \approx 0$ are expected for magnetic fields generated in an inflationary scenario [18, 19]. The dissipation scale, k_{diss} is not an independent parameter and should, in principle, be dependent on the amplitude and the shape of the magnetic fields spectrum. As in [42], we assume that k_{diss} is determined by damping into Alfvén waves [44, 45] and can be related to B_{eff} as

$$\frac{k_{\text{diss}}}{1 \text{ Mpc}^{-1}} \approx 1.4 h^{1/2} \left(\frac{10^{-7} \text{ Gauss}}{B_{\text{eff}}} \right) , \quad (5)$$

where B_{eff} is defined as the effective homogeneous field strength that would have the same total magnetic energy density. It is related to $\Omega_{B\gamma}$ via [42]

$$B_{\text{eff}} = 3.25 \times 10^{-6} \sqrt{\Omega_{B\gamma}} \text{ Gauss} . \quad (6)$$

Subsequently, the dissipation scale can be expressed in terms of $\Omega_{B\gamma}$ as

$$k_{\text{diss}} \approx 0.43 \sqrt{\frac{10^{-2}h}{\Omega_{B\gamma}}} \text{ Mpc}^{-1}. \quad (7)$$

One should be aware of the very approximate nature of the relations (5) and (7). They are based on the analysis in Ref. [44] where small perturbations on top of a homogeneous magnetic field were treated. To extend this analysis to a stochastic magnetic field with little power on long wavelengths, Ref. [45] introduced a smoothing procedure and split the spectrum into a ‘‘homogeneous’’ part and a ‘‘perturbations’’ part. It is not clear to us if this procedure is valid for an arbitrary spectrum, $S(k)$. Instead, we will use Eq. (5) as an approximate expression for the dissipation scale. We note that this relation also imposes an upper bound on k_I , since k_I cannot be greater than k_{diss} .

In practice, both scales (k_I and k_{diss}) that appear in the definition of the magnetic spectrum (3) are likely to be smaller than the resolution scale of a realistic CMB experiment. This means that only the large scale tail of the spectrum, *i.e.* the $0 < k < k_I$ range, will be relevant for calculating the shapes of the CMB correlation functions on the observable scales. The existence of the intermediate range $k_I < k < k_{\text{diss}}$ and the exponent n' will affect the inferred constraints on $\Omega_{B\gamma}$ only through an overall rescaling. For this reason, in the calculation of the CMB correlations, we will set $k_I = k_{\text{diss}}$, with k_{diss} given by (7), and work with a single power law spectrum

$$\tilde{\Delta}_M^2(k) = \begin{cases} \tilde{\Delta}_0^2 \left(\frac{k}{k_{\text{diss}}}\right)^{2n} & 0 < k < k_{\text{diss}} \\ 0 & k > k_{\text{diss}} \end{cases}, \quad (8)$$

where

$$\tilde{\Delta}_0^2 = 1.1 \times 10^4 \tilde{\Omega}_{B\gamma} \times \left(\frac{2n}{5}\right) \left(\frac{90 \text{ GHz}}{\nu_0}\right)^4 \quad (9)$$

The bound we obtain on $\tilde{\Omega}_{B\gamma}$ can then be easily converted to the bound on $\Omega_{B\gamma}$ via

$$\Omega_{B\gamma} = \tilde{\Omega}_{B\gamma} \kappa \left(\frac{k_I}{k_{\text{diss}}}\right)^{2n}. \quad (10)$$

We calculate the FR power spectrum as [42]

$$C_L^{\alpha\alpha} = \frac{2}{\pi} \int \frac{dk}{k} \tilde{\Delta}_M^2(k) \left[\frac{L}{2L+1} (\mathcal{T}_{L-1}(k))^2 + \frac{L+1}{2L+1} (\mathcal{T}_{L+1}(k))^2 - (\mathcal{T}_L^{(1)}(k))^2 \right], \quad (11)$$

where $\mathcal{T}_L(k)$ are transfer functions that are independent of the magnetic field:

$$\begin{aligned} \mathcal{T}_L(k) &\equiv \int_{\eta_*}^{\eta_0} d\eta \dot{\tau}(\eta) j_L(k(\eta_0 - \eta)) \\ \mathcal{T}_L^{(1)}(k) &\equiv \int_{\eta_*}^{\eta_0} d\eta \dot{\tau}(\eta) j_L'(k(\eta_0 - \eta)). \end{aligned} \quad (12)$$

Here η_* is the epoch at which the visibility function is maximum, j_L are the spherical Bessel functions, and $\dot{\tau}$ can be easily obtained numerically using public codes such as CMBFAST [46] or CAMB [47].

III. THE MODE COUPLING ESTIMATOR AND THE B -MODE SPECTRUM

FR will rotate the CMB polarization fields generated at last scattering. This introduces coupling between different CMB modes which can, in fact, be used to reconstruct the rotation angle map from the observed CMB polarization maps [39, 41, 48, 49]. Let $\tilde{T}(\hat{\mathbf{n}})$, $\tilde{Q}(\hat{\mathbf{n}})$ and $\tilde{U}(\hat{\mathbf{n}})$ be the un-rotated CMB temperature field and the two linear polarization Stokes parameters at angular position $\hat{\mathbf{n}}$. The temperature is not affected by FR, except for the depolarization effect [50] which would appear as a next order correction and can be ignored in our analysis. Under a rotation of the polarization by an angle $\alpha(\hat{\mathbf{n}})$, the two Stokes parameters transform like a spin two field. Thus, the observed fields are

$$(Q(\hat{\mathbf{n}}) \pm iU(\hat{\mathbf{n}})) = (\tilde{Q}(\hat{\mathbf{n}}) \pm \tilde{U}(\hat{\mathbf{n}})) \exp(\pm 2i\alpha(\hat{\mathbf{n}})). \quad (13)$$

The observed Stokes parameters can be further combined to form parity-even (E -mode) and parity-odd (B -mode) combinations which, in the flat sky approximation [32–34] are defined by

$$[E \pm iB](\mathbf{l}) = \int d\hat{\mathbf{n}} [Q(\hat{\mathbf{n}}) \pm iU(\hat{\mathbf{n}})] e^{\mp 2i\varphi_1} e^{-i\hat{\mathbf{l}} \cdot \hat{\mathbf{n}}}, \quad (14)$$

where $\varphi_1 = \cos^{-1}(\hat{\mathbf{n}} \cdot \hat{\mathbf{l}})$. The relevant² ensemble averages of the un-rotated CMB fields can be encapsulated in

$$\langle \tilde{x}(\mathbf{l}) \rangle = 0, \quad \langle \tilde{x}^*(\mathbf{l}) \tilde{x}'(\mathbf{l}') \rangle = (2\pi)^2 \delta(\mathbf{l} - \mathbf{l}') \tilde{C}_1^{xx'}, \quad (15)$$

where \tilde{x}, \tilde{x}' run over the T, E , or B fields, and $\tilde{C}_1^{xx'}$ are the un-rotated CMB power spectra.

We would like to isolate the effect of FR on the various correlators that describe the CMB. In particular, gravitational lensing causes CMB distortions that can interfere with the computation of the FR effect³. The change due to FR is the difference between lensed rotated fields and lensed un-rotated fields $\tilde{T}, \tilde{E}, \tilde{B}$. The change in the CMB fields $\delta x(l) = x(l) - \tilde{x}(l)$ due to FR is

$$\begin{aligned} \delta T(\mathbf{l}) &= 0, \\ \delta B(\mathbf{l}) &= 2 \int \frac{d^2 l'}{(2\pi)^2} [\tilde{E}(\mathbf{l}') \cos 2\varphi_{l1} - \tilde{B}(\mathbf{l}') \sin 2\varphi_{l1}] \alpha(\mathbf{L}), \\ \delta E(\mathbf{l}) &= -2 \int \frac{d^2 l'}{(2\pi)^2} [\tilde{B}(\mathbf{l}') \cos 2\varphi_{l1} + \tilde{E}(\mathbf{l}') \sin 2\varphi_{l1}] \alpha(\mathbf{L}), \end{aligned} \quad (16)$$

where $\mathbf{L} = \mathbf{l} - \mathbf{l}'$, and $\varphi_{l1} = \varphi_1 - \varphi_{l'}$. Thus, due to FR, a mode of wavevector \mathbf{L} mixes the polarization modes of wavevectors \mathbf{l} and $\mathbf{l}' = \mathbf{l} - \mathbf{L}$.

Let us take the ensemble average over multiple realizations of the unrotated CMB fields, while assuming a fixed α field. Then, for the rotated variables $x \neq x'$, one can write

$$\langle x^*(\mathbf{l}) x'(\mathbf{l}') \rangle_{\text{CMB}} = f_{xx'}(\mathbf{l}, \mathbf{l}') \alpha(\mathbf{L}), \quad (17)$$

where $f_{TB} = 2\tilde{C}_l^{TE} \cos 2\varphi_{l1}$, and $f_{EB} = 2[\tilde{C}_l^{EE} - \tilde{C}_l^{BB}] \cos 2\varphi_{l1}$. Namely, a single realization of a random rotation field α will induce parity-odd correlations of types TB and EB that are linearly proportional to the FR angle. If we also average over an ensemble of magnetic fields, the above two point functions will vanish for $x \neq x'$, since the expectation value of the magnetic field is zero.

The mode-coupling rotation (17) imprinted in the CMB by FR implies that one can build estimators for reconstructing the FR field from the observed CMB. Following Ref. [39–41, 49, 51], we can define an unbiased estimator $\hat{\alpha}_{xx'}(\mathbf{L})$ for $\alpha(\mathbf{L})$, where $x \neq x'$, by taking quadratic combinations of different polarization modes weighted by a factor $F_{xx'}(\mathbf{l}_1, \mathbf{l}_2)$:

$$\hat{\alpha}_{xx'}(\mathbf{L}) = N_L^{xx'} \int \frac{d^2 l_1}{(2\pi)^2} x(\mathbf{l}_1) x'(\mathbf{L} - \mathbf{l}_1) F_{xx'}(\mathbf{l}_1, \mathbf{L} - \mathbf{l}_1), \quad (18)$$

where $\mathbf{L} = \mathbf{l}_2 - \mathbf{l}_1$, and the normalization

$$N_L^{xx'} = \left[\int \frac{d^2 l_1}{(2\pi)^2} f_{xx'}(\mathbf{l}_1, \mathbf{L} - \mathbf{l}_1) F_{xx'}(\mathbf{l}_1, \mathbf{L} - \mathbf{l}_1) \right]^{-1}, \quad (19)$$

is chosen to make the estimator unbiased, i.e. $\langle \hat{\alpha}(\mathbf{L}) \rangle_{\text{CMB}} = \alpha(\mathbf{L})$. The fields $x(\mathbf{l})$ can be obtained from the map of an experiment, while the CMB power spectrum of un-rotated but lensed fields can be computed from publicly available Boltzmann codes like CMBfast [46] and CAMB [47]. The weights $F_{xx'}$ are determined by minimizing the variance subject to the normalization constraint. For $xx' = TB$ and EB the minimization yields

$$F_{xx'}(\mathbf{l}_1, \mathbf{l}_2) = \frac{f_{xx'}(\mathbf{l}_1, \mathbf{l}_2)}{C_{l_1}^{xx} C_{l_2}^{x'x'}}, \quad (20)$$

² We assume that the unrotated CMB temperature and polarization fluctuations are Gaussian distributed.

³ In this paper we do not utilize the frequency dependence of the FR as a tool to differentiate it from other effects.

where $C_{l_2}^{xx}$ and $C_{l_2}^{x'x'}$ are the observed power spectra including the effects of both the signal and the instrument

$$C_l^{xx} = \tilde{C}_l^{xx} + \Delta_x^2 e^{l^2 \theta_{\text{FWHM}}^2 / (8 \ln 2)} \quad (21)$$

where Δ_x is the detector noise and θ_{FWHM} is the full-width half-maximum (FWHM) resolution of the Gaussian beam [52].

The variance of the estimator can be calculated as

$$\begin{aligned} \text{Var}(\hat{\alpha}_{xx'}(\mathbf{L})) &= \langle \hat{\alpha}_{xx'}(\mathbf{L}) \hat{\alpha}_{xx'}^*(\mathbf{L}') \rangle \\ &= N_L^{xx'} N_{L'}^{xx'} \int \frac{d^2 l_1}{(2\pi)^2} \int \frac{d^2 l_2}{(2\pi)^2} \langle x(\mathbf{l}_1) x'(\mathbf{L} - \mathbf{l}_1) x(\mathbf{l}_2) x'(\mathbf{L}' - \mathbf{l}_2) \rangle F_{xx'}(\mathbf{l}_1, \mathbf{L} - \mathbf{l}_1) F_{xx'}(\mathbf{l}_2, \mathbf{L}' - \mathbf{l}_2) \\ &= (2\pi)^2 \delta(\mathbf{L} - \mathbf{L}') \{ C_L^{\alpha\alpha} + N_L^{xx'} \}. \end{aligned} \quad (22)$$

In the last line, the first term is the desired FR power spectrum and the second term is the noise – also referred to as the Gaussian noise – in the reconstruction of FR. Note that the noise turns out to coincide with the normalization of the minimum variance estimator as given by Eq. (19) [39, 41, 48, 49], and is independent of FR. In principle, there are higher order noise terms (referred to as non-Gaussian noise terms) which depend on FR, however, these terms are sub-dominant in comparison to the Gaussian noise. The signal-to-noise for detecting a spatially varying FR angle $\alpha(\hat{\mathbf{n}})$ using the estimator (18) is given by [39, 40]

$$\left(\frac{S}{N} \right)_{xx'}^2 = \sum_{l=2}^{l_{\text{max}}} \frac{f_{\text{sky}}}{2} (2l+1) \left(\frac{C_l^{\alpha\alpha}}{N_l^{xx'}} \right)^2, \quad (23)$$

where $C_l^{\alpha\alpha}$ is the rotation angle power spectrum, and we ignore the contribution of $C_l^{\alpha\alpha}$ to the variance (22) as it is negligible compared to $N_l^{xx'}$.

We also consider the case when $x = x' = B$, and the resultant BB correlation is quadratic in the rotation field. Averaging over the ensemble of magnetic fields gives the FR induced CMB B -mode power spectrum:

$$C_L^{BB} = 4 \int \frac{d^2 \mathcal{Y}}{(2\pi)^2} C_l^{\alpha\alpha} C_{l''}^{EE} \cos^2[2\varphi_{l''\mathbf{L}}] \Big|_{l''=\mathbf{L}-\mathbf{l}} \quad (24)$$

The signal-to-noise in this case (accounting for the B -modes from weak lensing but assuming no contribution from inflationary gravity waves) is given by

$$\left(\frac{S}{N} \right)_{BB}^2 = \sum_{l=2}^{l_{\text{max}}} \frac{f_{\text{sky}}}{2} (2l+1) \left(\frac{C_l^{BB}}{\mathcal{N}_l^{BB}} \right)^2, \quad (25)$$

where $\mathcal{N}_l^{BB} = C_l^{BB, \text{lensing}} + C_l^{BB, \text{noise}}$ and the noise power spectrum is $C_l^{BB, \text{noise}} = \Delta_P^2 \exp(l^2 \theta_{\text{FWHM}}^2 / 8 \ln 2)$, where Δ_P is the instrument noise for polarization.

One might wonder if gravitational lensing, which also generates off-diagonal correlations in the CMB with a leading order contribution to the trispectrum, might bias the mode coupling FR estimator (18). However, it has been shown that the effects of gravitational lensing and rotation are orthogonal and hence lensing does not bias estimates of rotation [40, 41]. Lensing does, however, increase the variance of the estimator, i.e. the Gaussian noise given by Eq. (19) is enhanced. For example, the noise of the EB estimator, N_ℓ^{EB} , depends on the observed CMB E and B mode power spectra, and is an integration over $(C_\ell^{EE} + \mathcal{N}_\ell^{EE})(C_\ell^{BB} + \mathcal{N}_\ell^{BB})$. Further, the B -modes due to lensing scale as white noise up to $l \sim 1000$, and correspond to a noise level of $5\mu\text{K-arcmin}$. Therefore, the increase in the variance is sub-dominant for experiments with $\Delta_P > 5\mu\text{K-arcmin}$. However, for small instrumental noise, $\Delta_P \leq 5\mu\text{K-arcmin}$, lensing B -modes become important, saturating the variance to $\sim 10^{-6} \text{ deg}^2$ even for an ideal experiment.

In the next section, we compare detectability of the FR signal in upcoming and future CMB maps with the mode-coupling estimators (18) vs. using the B -mode spectrum (24). Interestingly, we find that one method can out-perform the other depending on the value of the magnetic spectral index.

IV. DETECTABILITY OF PRIMORDIAL MAGNETIC FIELDS

To forecast the detectability of FR we consider three experimental setups: a Planck-like satellite [53] (E1), a ground-or balloon-based experiment realistically achievable in the next decade (E2), and a future dedicated CMB polarization satellite (E3). We will adopt the following parameters for the three experiments:

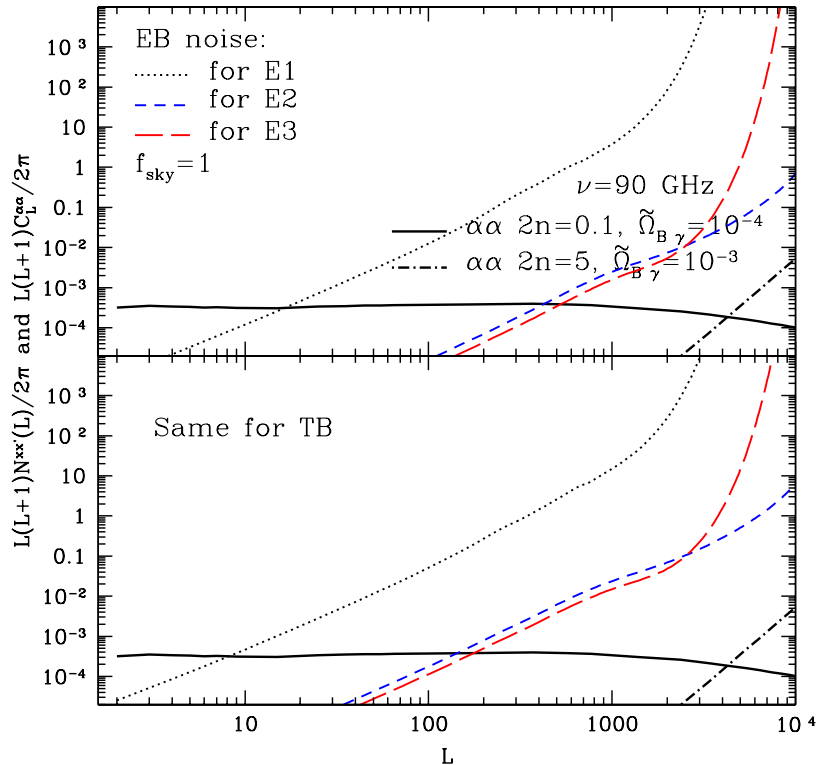


FIG. 1: The noise $L(L+1)N_L^{xx'}/2\pi$ as given by Eq. (19) for the *EB* (upper panel) and *TB* (lower panel) estimators as a function of multipole L for three experimental setups (E1, E2, E3). Also plotted is the FR power spectrum $L(L+1)C_L^{\alpha\alpha}/2\pi$ for the causal magnetic spectrum with $2n=5$ and for a nearly scale invariant spectrum with $2n=0.1$. The amplitude of the FR spectrum is set by the observed frequency of $\nu_0=90$ GHz and $\tilde{\Omega}_{B\gamma}=10^{-3}$ for the causal case ($2n=5$), and $\tilde{\Omega}_{B\gamma}=10^{-4}$ for the nearly scale invariant case ($2n=0.1$).

- E1: a Planck-like satellite [53] with noise level $\Delta_P = 60\mu K\text{-arcmin}$ and $\Theta_{\text{FWHM}} = 7'$
- E2: a next decade sub-orbital experiment with $\Delta_P = 3.0\mu K\text{-arcmin}$ and $\Theta_{\text{FWHM}} = 1'$
- E3: a CMBPol-like instrument with $\Delta_P = \sqrt{2}\mu K\text{-arcmin}$ and $\Theta_{\text{FWHM}} = 4'$, typical of the proposed future space-based CMB experiments [54, 55]

The forecasts directly depend on the fraction of the sky covered by the experiment, f_{sky} , which is close to unity for E1 and E3, and will be smaller for E2. We quote our bounds subject to specifying f_{sky} which only appears under a quartic root in the bounds on B_{eff} .

In Fig. 1 we plot $L(L+1)N_L^{xx'}/2\pi$ vs multipole L with the noise for the *EB* and *TB* estimators given by Eq. (19) for experiments E1, E2 and E3, along with the FR spectrum $L(L+1)C_L^{\alpha\alpha}/2\pi$ for two choices of the magnetic spectral index $2n$. The amplitudes of the rotation spectra are normalized to $\tilde{\Omega}_{B\gamma} = 10^{-3}$ for the causal case ($2n=5$) and $\tilde{\Omega}_{B\gamma} = 10^{-4}$ for the nearly scale invariant case ($2n=0.1$), with $\tilde{\Omega}_{B\gamma}$ related to $\Omega_{B\gamma}$ via Eq. (10). For all the estimates in this paper we adopted an observational frequency of $\nu_0=90$ GHz, but one can easily scale the signal to other frequencies using Eq. (9). For all three experiments under consideration, the *EB* estimator is more sensitive than the *TB*, with the noise $N_L^{xx'}$ staying roughly constant up to $L \sim 1000$. Although we do not show $L=0$ in the plot, these estimators can also be used to estimate the detectability of uniform rotation.

In Fig. 2 we plot the noise contribution to the variance of the *B*-mode spectrum, along with the FR induced *B*-mode spectrum for $\tilde{\Omega}_{B\gamma} = 10^{-3}$ for $2n=5$, and $\tilde{\Omega}_{B\gamma} = 10^{-4}$ for $2n=0.1$. In the latter case, the shape of the *B*-mode spectrum is a close copy of the underlying *E*-mode, except that the FR induced spectrum falls off as $L(L+1)C_L^{BB} \propto L^{2n-1}$ at high L [42, 56] compared to the exponential fall off of the primordial *E*-mode. The L^{2n-1} tail implies a sharply rising spectrum for the causal case with ($2n=5$), with most of the power concentrated near the dissipation scale $L_{\text{diss}} \sim 10^4 \text{ Mpc} \times k_{\text{diss}}$.

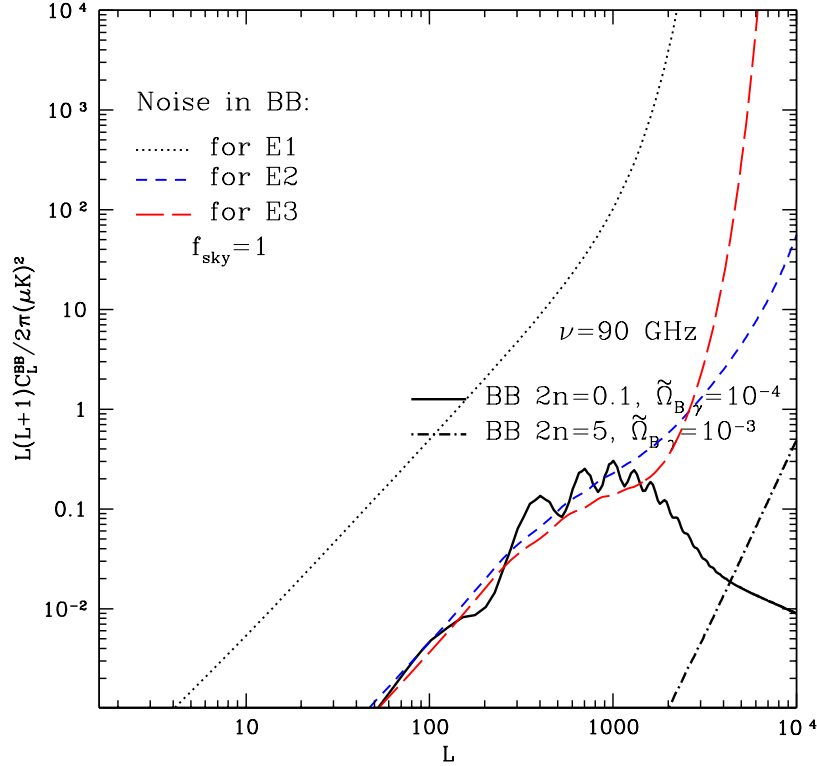


FIG. 2: The B -mode polarization pixel noise, $L(L+1)C_L^{BB,\text{noise}}/2\pi$, for experiments E1, E2, and E3 as a function of multipole L . Also shown is the B -mode spectrum induced by FR for a causal magnetic spectrum with $2n = 5$ and for a nearly scale invariant spectrum with $2n = 0.1$. The observed frequency is set to $\nu_0 = 90 \text{ GHz}$, $\tilde{\Omega}_{B\gamma} = 10^{-3}$ for the causal case, and $\tilde{\Omega}_{B\gamma} = 10^{-4}$ for the scale invariant case.

To forecast the minimum detectable magnetic field energy fraction, we define it as $\tilde{\Omega}_{B\gamma}$ for which S/N in Eqs. (23) and (25) is unity. Note that $\tilde{\Omega}_{B\gamma}$ determines the dissipation scale k_{diss} via Eq. (7). We perform this forecast for each estimator, for different experiments, and for several choices of $2n$. We restrict the maximum multipole to $L_{\text{max}} = 10000$. Fig. 3 shows the minimum detectable $\tilde{\Omega}_{B\gamma}$ as a function of the instrument noise Δ_P for a fixed beam $\Theta_{\text{FWHM}} = 8'$ for two choices of $2n$. As one can see, at high noise levels ($\Delta_P \gtrsim 100 \mu\text{K}\cdot\text{arcmin}$), the B -mode power spectrum tends to either give comparable or better constraints than the EB estimator. In particular, it is always the better probe of the causal primordial magnetic fields. However, for upcoming polarization sensitive experiments with lower levels of noise, the EB estimator will become almost comparable to the B -mode power spectrum for causal fields, and outperform it when probing scale-invariant FR fields.

In Fig. 4 we plot the minimum $\tilde{\Omega}_{B\gamma}$ that will be detectable by the E1, E2 and E3 experiments depending on the value of the magnetic spectral index $2n$. We see that for all experiments, the EB estimator begins to outperform the B -mode spectrum when $2n \lesssim 1$, while the TB estimator is always the third best.

The relative strengths of the three estimators, demonstrated in Figs. 3 and 4, can be understood as follows. Generally, the EB and TB estimators have a larger number of independent modes contributing to the signal than the B -mode spectrum. Thus, in principle, it is not surprising if they result in a higher signal to noise. However, whether that is the case depends on the experimental noise level, and the distribution of power in the given combination of CMB fields and in the magnetic field. For a scale-invariant PMF spectrum, the B -mode is essentially a copy of the E -mode, with most of the B -mode power being on scales where the E -modes are also most prominent. This results in a strong correlation between E and B for scale-invariant fields. In the case of the TB correlation, the underlying T and E (B is obtained by a scale-invariant rotation of E) fields peak on rather different scales. Namely, T peaks at $\ell \sim 200$ while E peaks at $\ell \sim 1000$. In other words, the intrinsic correlation between T and E is already suboptimal, translating into a lesser correlation between T and B . Thus, for experiments with a sufficiently low noise Δ_P , such as E1, E2 and E3 considered in this paper, the EB estimator performs better than TB for scale-invariant fields. This would not necessarily remain true if polarization measurements had a significantly higher experimental noise.

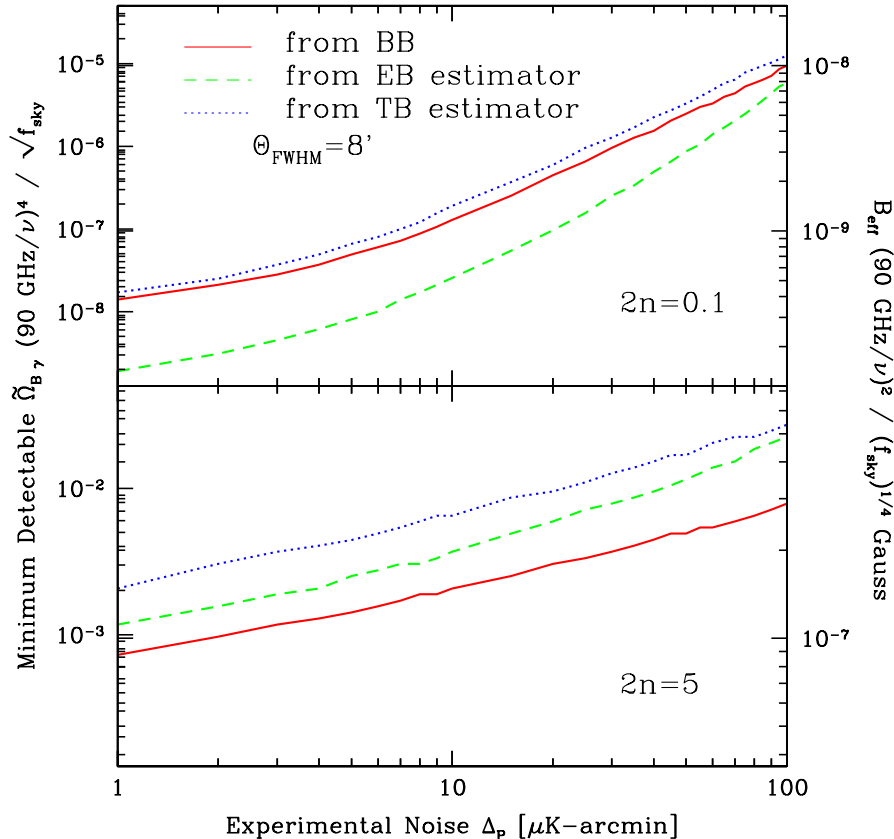


FIG. 3: Comparison of the three estimators, BB (solid red), EB (dashed green) and TB (dotted blue). Plotted is the minimum detectable magnetic field amplitude $\tilde{\Omega}_{B\gamma}$ as a function of the experimental noise, with $\Theta_{\text{FWHM}} = 8'$. The upper panel is for the nearly scale invariant case with $2n = 0.1$, while the lower panel is for the causal case with $2n = 5$.

For the blue causal spectra, the FR power is concentrated on very small scales, far away from the scales at which any of the unrotated CMB fields have significant power. This means that the B -modes in the observable range are obtained either by the rotation of E -modes far away from their peak power scale, or by a rotation of peak E -mode by a negligible angle. This means that E and B fields peak at very different scales, with their correlation being close to zero over the observable scales. In this case, we see that the B -mode spectrum, i.e. the BB correlation, has the highest signal to noise.

When interpreting the forecasted bounds on the magnetic field energy fraction or the effective magnetic field strength in Figs. 3 and 4, several points must be kept in mind:

1. The constraints are on $\tilde{\Omega}_{B\gamma}$, obtained after setting $k_I = k_{\text{diss}}$, with the dissipation scale determined from Eq. (7). For scale-invariant fields there is no difference between $\tilde{\Omega}_{B\gamma}$ and $\Omega_{B\gamma}$, since the factor relating them in Eq. (10) goes to unity when $2n \rightarrow 0$. Also, for scale-invariant fields, the effective field B_{eff} defined via Eq. (6) is the same as the commonly used B_λ , which is the field smoothed on a given scale λ . Thus, our forecasts of the minimum detectable B_{eff} for scale-invariant fields can be directly compared to most other bounds in the literature.
2. For causal fields, the bound on $\tilde{\Omega}_{B\gamma}$ will generally overestimate the magnetic energy fraction, since it assumes that the spectrum will keep rising at the same steep rate ($2n = 5$) all the way to the dissipation scale, which is much smaller than the smallest scale directly probed by CMB experiments. Simulations [43] suggest that the spectrum must become less steep, with $2n' = 3$ in the range $k_I < k < k_{\text{diss}}$, implying a smaller net magnetic energy fraction $\Omega_{B\gamma}$. Since the value of k_I is not well-known at this point, we chose to quote our bounds in terms of $\tilde{\Omega}_{B\gamma}$, while keeping in mind that bounds on $\Omega_{B\gamma}$ for causal fields will generally be tighter.
3. Strictly speaking, our bounds are on the fraction in magnetic fields at the time when the initial conditions for the transfer functions (12) were set, which is a time close to last scattering. While it is expected that the magnetic

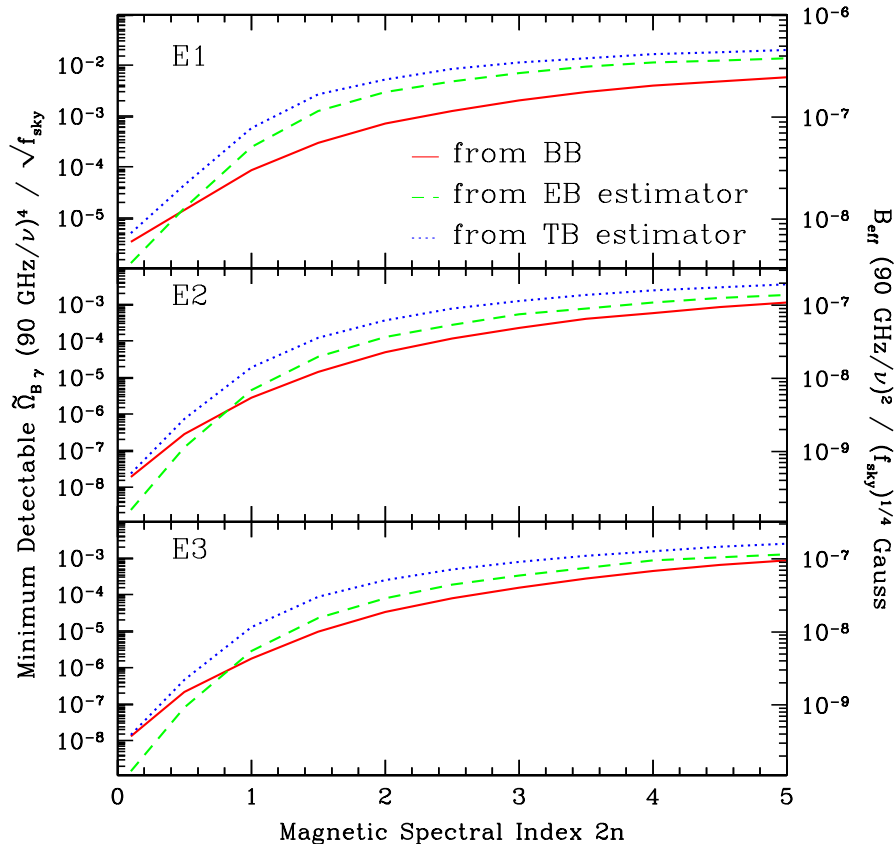


FIG. 4: The minimum detectable magnetic field amplitude $\tilde{\Omega}_{B\gamma}$ as a function of the magnetic spectral index $2n$ for the three estimators, *BB* (solid red), *EB* (dashed green) and *TB* (dotted blue). The top panel is for E1, the middle panel is for E2 and the lower panel is for E3.

fields are effectively frozen-in between the BBN and last scattering, with a relatively slow time evolution of the dissipation scale, this is still an approximation.

4. The bounds are based on using a single frequency band. Using several bands will improve the constraints.

Generally, CMB is not very sensitive to magnetic fields with blue spectra because most of the anisotropies are concentrated on very small scales. This is what Figs. 3 and 4 are showing too. However, looking for the FR signatures at many frequencies can potentially improve the existing CMB bounds on causal fields by a large factor. We leave this question as a topic for future exploration.

In the case of scale-invariant fields, current bounds on the magnetic field strength from WMAP are at a level of a few nG [25, 26, 28–30]. These bounds are based on the anisotropies induced by the metric fluctuations sourced by magnetic fields, and ignore the FR effect. In Refs. [27, 42] the WMAP bound using FR was obtained at the 10^{-7} G level. As one can see from Fig. 4, Planck (E1) can almost match today’s bounds for scale invariant ($n = 0$) fields using the *EB* estimator at only one frequency, while future probes, such as E2 and E3, can improve the bounds by an order of magnitude! This suggests that the mode coupling estimators of FR will be a very powerful, if not the most powerful, direct probe of scale-invariant magnetic fields at the time of last scattering.

V. SUMMARY

A primordial magnetic field present at and just after last scattering will Faraday-rotate the plane of polarization of the CMB photons. The FR will create *B*-mode polarization even in the absence of primordial sources, such as gravity waves. In addition to a *B*-mode autocorrelation, FR also couples different modes of the CMB fields, generating specific off-diagonal correlators. Estimators of the polarization rotation angle, such as (18), can utilize these non-Gaussian

features to reconstruct the FR map. One can construct four such estimators containing products of two CMB fields, one of which contains polarization: TE , EE , TB , and EB . Of these four, the first two receive a large contribution to their variance from the usual scalar adiabatic Gaussian perturbations which makes it harder to find the FR signal. In this paper, we have considered the last two and found that the EB estimator has the highest signal-to-noise.

For causal magnetic fields, which tend to have very blue power spectra, the B -mode power spectrum has a higher signal-to-noise due to reasons explained in the previous section. However, the EB estimator performs better for scale-invariant fields. In addition, there are certain advantages in using mode-coupling based estimators, such as EB , over the traditional B -modes power spectrum. For instance, there are other sources that can generate B -modes, such as weak lensing, patchy reionization, inflationary tensor perturbations or cosmic strings, and, in fact, metric perturbations induced by the magnetic fields. Hence, one has to separate the FR induced B -modes either by using the frequency dependence of FR or features in the B -mode spectrum. Interestingly, while patchy reionization and lensing also generate off-diagonal correlations in CMB, their contributions are “orthogonal” to the features imprinted by FR [49]. Hence, mode-coupling estimators do not suffer from contamination from other contributions. This means that a larger part of the information in the frequency dependence can be used for systematic checks and to separate from other foreground contamination. In addition, mode-coupling estimators can be used to reconstruct the map of FR. This FR map can be used to cross-correlate with other tracers of magnetic fields, including CMB maps and surveys of large scale structure. Such correlations studies are useful for systematic checks and for increasing the signal-to-noise.

We have found that a Planck-like experiment at 90GHz can detect scale-invariant PMF of a few nG strength, which is comparable to the \sim nG sensitivity forecasted for Planck based on information in the CMB temperature anisotropies [28]. Future CMB experiments will be able detect scale-invariant fields as weak as 10^{-10} G at 90GHz. Thus, FR should become a leading diagnostic of PMF when analyzing future CMB polarization data.

Acknowledgments

APSY gratefully acknowledges funding support from NASA award number NNX08AG40G and NSF grant number AST-0807444. LP is supported by a Discovery Grant from the Natural Sciences and Engineering Research Council of Canada. TV is supported by the Department of Energy at ASU, and is grateful to the Institute for Advanced Study, Princeton for hospitality. We thank Soma De for pointing out inconsistencies in the noise plots in Figs 1 and 2 that appeared in an earlier version of the manuscript, that we have subsequently corrected.

-
- [1] L. M. Widrow, Rev. Mod. Phys. **74**, 775 (2002).
 - [2] A. Neronov and I. Vovk, Science **328**, 73 (2010), 1006.3504.
 - [3] K. Dolag, M. Kachelriess, S. Ostapchenko, and R. Tomas, Astrophys.J. **727**, L4 (2011), 1009.1782.
 - [4] A. Taylor, I. Vovk, and A. Neronov, Astron.Astrophys. **529**, A144 (2011), 1101.0932.
 - [5] I. Vovk, A. M. Taylor, D. Semikoz, and A. Neronov (2011), 1112.2534.
 - [6] S. Ando and A. Kusenko, Astrophys.J. **722**, L39 (2010), 1005.1924.
 - [7] A. E. Broderick, P. Chang, and C. Pfrommer, Astrophys.J. **752**, 22 (2012), 1106.5494.
 - [8] D. Miniati and A. Elyiv, arXiv:astro-ph/1208.1761.
 - [9] D. Grasso and H. R. Rubinstein, Physics Reports **348**, 163 (2001), arXiv:astro-ph/0009061.
 - [10] T. Vachaspati, Phys.Lett. **B265**, 258 (1991).
 - [11] J. M. Cornwall, Phys. Rev. **D56**, 6146 (1997), hep-th/9704022.
 - [12] T. Vachaspati, Phys. Rev. Lett. **87**, 251302 (2001), astro-ph/0101261.
 - [13] J. Garcia-Bellido, M. Garcia-Perez, and A. Gonzalez-Arroyo, Phys. Rev. **D69**, 023504 (2004), hep-ph/0304285.
 - [14] C. J. Copi, F. Ferrer, T. Vachaspati, and A. Achucarro, Phys. Rev. Lett. **101**, 171302 (2008), 0801.3653.
 - [15] T. Vachaspati, Phil. Trans. Roy. Soc. Lond. **A366**, 2915 (2008), 0802.1533.
 - [16] Y. Ng and T. Vachaspati, Phys. Rev. **D82**, 023008 (2010), 1001.4817.
 - [17] Y. Chu, J. Dent, and T. Vachaspati, ArXiv e-prints (2011), 2011.
 - [18] M. S. Turner and L. M. Widrow, Phys. Rev. **D37**, 2743 (1988).
 - [19] B. Ratra, Astrophys. J. **391**, L1 (1992).
 - [20] J. Matese and R. O’Connell, Nature **222**, 649 (1969).
 - [21] P. J. Kernan, G. D. Starkman, and T. Vachaspati, Phys. Rev. D **54**, 7207 (1996), arXiv:astro-ph/9509126.
 - [22] B.-l. Cheng, A. V. Olinto, D. N. Schramm, and J. W. Truran, Phys.Rev. **D54**, 4714 (1996), astro-ph/9606163.
 - [23] D. Grasso and H. R. Rubinstein, Phys.Lett. **B379**, 73 (1996), astro-ph/9602055.
 - [24] M. Kawasaki and M. Kusakabe (2012), 1204.6164.
 - [25] F. Finelli, F. Paci, and D. Paoletti, Phys. Rev. **D78**, 023510 (2008), 0803.1246.

- [26] D. Paoletti, F. Finelli, and F. Paci, *Mon. Not. Roy. Astron. Soc.* **396**, 523 (2009), 0811.0230.
- [27] T. Kahniashvili, Y. Maravin, and A. Kosowsky, *Phys. Rev. D* **80**, 023009 (2009), 0806.1876.
- [28] D. Paoletti and F. Finelli, *Phys.Rev.* **D83**, 123533 (2011), 1005.0148.
- [29] T. Seshadri and K. Subramanian, *Phys.Rev.Lett.* **103**, 081303 (2009), 0902.4066.
- [30] P. Trivedi, T. Seshadri, and K. Subramanian, *Phys.Rev.Lett.* **108**, 231301 (2012), 1111.0744.
- [31] A. Kosowsky and A. Loeb, *Astrophys.J.* **469**, 1 (1996), astro-ph/9601055.
- [32] M. Kamionkowski, A. Kosowsky, and A. Stebbins, *Phys.Rev.Lett.* **78**, 2058 (1997), astro-ph/9609132.
- [33] U. Seljak and M. Zaldarriaga, *Phys. Rev. Lett.* **78**, 2054 (1997).
- [34] M. Kamionkowski, A. Kosowsky, and A. Stebbins, *Phys. Rev. D* **55**, 7368 (1997).
- [35] R. Crittenden, R. L. Davis, and P. J. Steinhardt, *Astrophys.J.* **417**, L13 (1993), astro-ph/9306027.
- [36] U. Seljak, U.-L. Pen, and N. Turok, *Phys.Rev.Lett.* **79**, 1615 (1997), astro-ph/9704231.
- [37] T. Kahniashvili and B. Ratra, *Phys.Rev.* **D71**, 103006 (2005), astro-ph/0503709.
- [38] K. E. Kunze, *Phys.Rev.* **D85**, 083004 (2012), 1112.4797.
- [39] M. Kamionkowski, *Phys.Rev.Lett.* **102**, 111302 (2009), 0810.1286.
- [40] A. P. S. Yadav, R. Biswas, M. Su, and M. Zaldarriaga, *Phys. Rev. D* **79**, 123009 (2009), 0902.4466.
- [41] V. Gluscevic, M. Kamionkowski, and A. Cooray, *Phys. Rev. D* **80**, 023510 (2009), 0905.1687.
- [42] L. Pogosian, A. P. Yadav, Y.-F. Ng, and T. Vachaspati, *Phys.Rev.* **D84**, 043530 (2011), 1106.1438.
- [43] K. Jedamzik and G. Sigl, *Phys.Rev.* **D83**, 103005 (2011), 1012.4794.
- [44] K. Jedamzik, V. Katalinic, and A. V. Olinto, *Phys. Rev.* **D57**, 3264 (1998), astro-ph/9606080.
- [45] T. Kahniashvili, A. G. Tevzadze, S. K. Sethi, K. Pandey, and B. Ratra, *Phys.Rev.* **D82**, 083005 (2010), 1009.2094.
- [46] U. Seljak and M. Zaldarriaga, *Astrophys. J.* **469**, 437 (1996), astro-ph/9603033.
- [47] A. Lewis, A. Challinor, and A. Lasenby, *Astrophys.J.* **538**, 473 (2000), astro-ph/9911177.
- [48] V. Gluscevic, D. Hanson, M. Kamionkowski, and C. M. Hirata (2012), 1206.5546.
- [49] A. P. S. Yadav, M. Su, and M. Zaldarriaga, *Phys. Rev. D* **81**, 063512 (2010), 0912.3532.
- [50] D. D. Harari, J. D. Hayward, and M. Zaldarriaga, *Phys.Rev.* **D55**, 1841 (1997), astro-ph/9608098.
- [51] W. Hu and T. Okamoto, *Astrophys. J.* **574**, 566 (2002).
- [52] D. J. Eisenstein, W. Hu, and M. Tegmark, *Astrophys.J.* **518**, 2 (1999), astro-ph/9807130.
- [53] (Planck Collaboration) (2006), astro-ph/0604069.
- [54] D. Baumann et al. (CMBPol Study Team), *AIP Conf.Proc.* **1141**, 10 (2009), 0811.3919.
- [55] F. Bouchet et al. (CORe Collaboration) (2011), 1102.2181.
- [56] A. Kosowsky, T. Kahniashvili, G. Lavrelashvili, and B. Ratra, *Phys. Rev. D* **71**, 043006 (2005).